

Bedding Dips from the CRP-3 Drillhole, Victoria Land Basin, Antarctica

R.D. JARRARD^{1*}, C.J. BÜCKER^{2,§}, T.J. WILSON³ & T.S. PAULSEN⁴

¹Dept. of Geology & Geophysics, 717 WBB, Univ. of Utah, 135 S. 1460 East, Salt Lake City UT 84112-0111 - U.S.A

²GGA, Leibniz Institute for Applied Geosciences, Stilleweg 2, 30655 Hannover - Germany

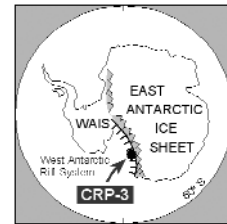
³Dept. of Geological Sciences, Ohio State University, 275 Mendenhall, 125 S. Oval Mall, Columbus OH 43210 - U.S.A

⁴Dept. of Geology, University of Wisconsin, Oshkosh, WI 54901 - U.S.A

[§]Present address: RWE-DEA AG, Ueberseering 40, 22297 Hamburg - Germany

Received 28 October 2000; accepted in revised form 6 December 2001

Abstract - Bedding dips in the CRP-3 drillhole were determined in three ways: (1) analysis of a dipmeter log, (2) identification of bed boundaries on borehole televiwer log images, and (3) identification of bed boundaries on digital images of the outer surfaces of oriented cores. All three methods determine both dip magnitude and downdip azimuth of bedding. Dipmeter results document variations in bedding dip throughout the logged interval (20-902 mbsf), whereas core and televiwer results are available at present only for selected depth intervals. Dipmeter data indicate that structural dip is remarkably constant, at 21° dip to azimuth 65°, throughout the Tertiary shelf section, except for the top 100 m where dips appear to be 5-10° shallower. This pattern, in conjunction with the systematically increasing dips throughout CRP-2A, suggests that the growth faulting active during CRP-2A deposition began during the final period of deposition at CRP-3. Normal faults at 260 and 539 mbsf in CRP-3 exhibit neither drag (localized dip steepening) nor significant changes in structural dip across them. Oriented core and televiwer analyses, covering a total of 200 m in the interval 400-900 mbsf, indicate bedding patterns that confirm the dipmeter results. The doleritic breccia at the base of the Tertiary section has steeper dips than overlying structural dips, possibly indicating a sedimentary dip to ENE in these fan sediments. Dip directions in the underlying Devonian Beacon sandstone are surprisingly similar to those in the overlying Tertiary section. Superimposed on the average Beacon dip of 22° to the ENE are localized tilts of up to 20°, probably caused by Tertiary fracturing and brecciation rather than original sedimentary dip variations.



INTRODUCTION

The Cape Roberts Project (CRP) is an international drilling project whose aim is to reconstruct Neogene to Palaeogene palaeoclimate and the tectonic history of the Transantarctic Mountains and West Antarctic rift system, by obtaining continuous cores and well logs from a site near Cape Roberts, Antarctica. Offshore Cape Roberts, tilting and erosion of strata have brought Lower Miocene to Lower Oligocene sediments near the seafloor. The three CRP holes penetrate successively older portions of a 1600 m composite stratigraphic sequence. CRP-2/2A depths can be converted to composite depth (CRP-1 standard) by adding 40 m, and CRP-3 depths can be converted by adding 680 m (Cape Roberts Science Team, 2000). CRP-3 cored 821 m of Lower Oligocene and possibly Upper Eocene sedimentary rocks and 116 m of underlying Beacon sandstone of Devonian age (Cape Roberts Science Team, 2000). Average core recovery was 97%. The mid-Tertiary section consists primarily of shelf sandstones and muddy sandstones; other lithologies include common thin conglomerate beds and less common sandy

mudstones and diamictites (Cape Roberts Science Team, 2000). Between the Tertiary shelf sediments and the Beacon sandstone is 34 m of doleritic breccia, mid-Tertiary in age.

This study determines bedding dips in the CRP-3 drillhole with three data sources: dipmeter logs, whole-core images, and borehole televiwer (BHTV) images. The main goal of this dip analysis is determination of structural dips, to identify tilting episodes and subtle angular unconformities. These three datasets are also used in several companion studies. Digital whole-core images were obtained at the drill site (Cape Roberts Science Team, 2000), primarily for structural analyses (Wilson & Paulsen, this volume). Jarrard, Paulsen & Wilson (this volume) compare whole-core and BHTV images to orient cores. The BHTV data are also used for stress analysis (Jarrard, Moos et al., this volume). Dipmeter and BHTV logs are two of several kinds of downhole logs run at CRP-3 (Cape Roberts Science Team, 2000); analyses of the other logs are presented by Bücker, Jarrard et al. (this volume) and by Bücker, Wonik & Jarrard (this volume).

*Corresponding author (jarrard@mail.mines.utah.edu)

DATA PROCESSING

LOGGING OPERATIONS AND ORIENTATION

CRP-3 was logged in three phases: the open-hole interval 346-20 mbsf was logged at the conclusion of drilling with HQ drillrod (96 mm hole diameter, 61 mm core diameter), the interval 770-346 mbsf was logged during drilling with NQ drillrod (76 mm hole diameter, 45 mm core diameter), and the interval 902-765 mbsf was logged at the conclusion of drilling. Two intervals were not logged because hole conditions were too unstable to risk losing the tools: the upper fault zone (256-272 mbsf), and the bottom part of the hole (902-939 mbsf), which was blocked by swelling clays in an altered intrusion.

The dipmeter and BHTV tools record azimuth and angle of borehole deviation. CRP-3 was nearly vertical: hole deviation was to the southwest, with a deviation angle of 1.0°-2.5° from vertical in the top 350 mbsf, and about 1.5° in the lower portion of the hole (Cape Roberts Science Team, 2000). Although this deviation is minor, dipmeter dips are corrected from borehole to *in situ* coordinates. Core and BHTV dips, in contrast, are not corrected.

The Antares® dipmeter and BHTV include three perpendicular magnetometers, for tool orientation. Two horizontal magnetometers provide a continuous record of orientation of each tool with respect to magnetic north, so that all data can be converted from tool coordinates to magnetic north. We converted the data from magnetic north to true north coordinates, using measurements of local deviation based on an on-ice reference magnetometer. The CRP-3 site is actually at a higher latitude than the South Magnetic Pole, and it is so close to the magnetic pole that we considered it necessary to test the 148.3° local deviation based on the International Geomagnetic Reference Field (IGRF). An additional concern at very high latitudes is that magnetic storms can cause sudden, large swings in local deviation. Consequently, the reference magnetometer recorded 3-component magnetic field direction throughout dipmeter and BHTV logging. Fortunately, magnetic storm activity was low during logging, causing declination variations of <3°. Our measurements with the reference magnetometer were consistent with the IGRF value: 147-148°. Local deviation was also measured with GPS surveys in August and October 1999. These measurements, 148.5° and 147.5°, are nearly identical to the IGRF prediction.

DIPMETER

CRP-3 was logged with an Antares® 4-pad, slimhole dipmeter. This tool measures resistivity at each pad at a 5-mm vertical spacing. Dipmeter processing steps, including gain adjustment, spike removal, pad equalization, and depth shifting, are

similar to those employed for CRP-2A and described by Jarrard et al. (2000). Thin conglomerates, which are relatively abundant, were deleted before dip analysis.

Lonestones are much less abundant at CRP-3 than at CRP-2A, so their associated resistivity spikes are less of a problem. To minimize the effects of lonestones and patchy cements on our dipmeter analyses, we employed two methods of spike removal. We subjectively edited all raw microresistivity traces, deleting high-resistivity spikes. We also used the objective spike detection algorithm of Jarrard et al. (2000). We found that the subjectively edited dataset gave a stabler, more consistent suite of dip determinations above 550 mbsf, whereas the objectively edited dataset was superior below 550 mbsf. For determination of bedding dips from the despiked dipmeter data, we used the program Ezdip®. Results depend on a variety of user-determined processing parameters. For the Tertiary sediments above 790 mbsf, we achieved the best signal-to-noise ratio with a window length of 0.25 m, a step increment of 0.12 m, and a correlation angle of 0-55°.

Except for occasional conglomerates, the Tertiary shelf sedimentary environment (0-789 mbsf) is generally favorable for dipmeter-based determination of bedding dips. In contrast, the underlying doleritic breccia and Beacon sandstone are challenging for dipmeter analysis, because many correlations among the four resistivity pads are attributable not to bedding but to brecciation or fracturing. Furthermore, the doleritic breccia has correlations from dolerite clasts and much of the unit is extensively faulted (Cape Roberts Science Team, 2000; Wilson & Paulsen, this volume). These problems can be reduced by processing changes such as increasing the window length substantially, assuming that only bedding will exhibit a parallel fabric over a wide interval. Nevertheless, spurious picks and unintentional picking on fracture sets are unavoidable. Our most robust solution in the breccia used a window length of 2 m, step length of 1 m, and scan angle of 80°. We processed the Beacon interval with both a restrictive parameter set (0.5 m, 0.25 m, 50°) and an inclusive one (0.25 m, 0.12 m, 50°).

CORE AND BOREHOLE TELEVIEWER

As part of the core processing flow at Cape Roberts Drillsite, both whole cores and split cores were routinely digitally imaged with a DMT Corescan® color scanner (Cape Roberts Science Team, 2000). Prior to core splitting, the outer surfaces of most cores were imaged; exceptions were cores with too little strength to be rotated on the scanner without breaking up. In many cases, it is possible to determine relative orientation among successive core

pieces and among successive core images, by matching and fitting together the broken core surfaces. This process can be undertaken with the whole-core images in a process referred to as “stitching”. Each interval of stitched-together images is a continuous composite with correct relative orientations among successive pieces. Seventeen intervals, totaling 231 m (25% of the cored interval), were stitched. These stitched intervals were then oriented with respect to a geographic (NESW) coordinate system, by comparing them to oriented BHTV images and rotating them to match orientations of fractures, bedding, and clasts (Jarrard, Paulsen & Wilson, this volume). Jarrard, Paulsen & Wilson (this volume) subjectively estimate the accuracy of orientation as $\pm 15^\circ$ for most stitched-core intervals and $\pm 25^\circ$ for individual features (such as beds) within each interval. Almost all of these stitched-core intervals were included in our studies of bedding dips. “Bedding” is here defined as a change in gray level, sinusoidal in shape on unwrapped 360° core or BHTV images, interpreted to be caused by a change in lithology or porosity. Fractures are readily distinguished from bedding within these images, and we exclude fractures from our analyses.

Core image processing and analysis techniques were generally similar to those described by Jarrard et al. (2000), except that Corelog® processing software was replaced with more versatile WellCAD®. Because our focus is on delineation of primary and structural dips, we exclude obvious soft-sediment deformation and lonestone sag and drape from our bedding picks. However, both can occur at a scale large enough to be unrecognized in the core images.

The BHTV is an acoustic instrument that provides an image of surface reflectivity of the wall of a fluid-filled hole (Zemanek et al., 1970). As the tool is pulled up the hole, a rotating transducer obtains continuous 360° images of both amplitude and traveltime. CRP-3 amplitude images were most useful for identification of geologic features such as fractures, bedding, and clasts. Reflection amplitude depends mainly on reflectivity and roughness of the borehole wall. Vertical resolution is 3 mm, and horizontal resolution is 2.5° or 5° , depending on data acquisition parameters. Hole size was quite uniform, based on dipmeter measurements (Cape Roberts Science Team, 2000). The CRP-3 BHTV logs, like other CRP-3 well logs, initially exhibited up to 2.5 m of depth shift compared to coring depths, caused mainly by stretch of the logging cable. After depth shifting (Jarrard, Moos et al., this volume), residual depth shifts are everywhere less than 10 cm. BHTV log quality varied from poor to excellent, generally improving with increasing depth. Much of the top half of the BHTV log provided only rare returns from the borehole wall, possibly because of mudcake. Our bedding analyses are therefore confined to the bottom half of the borehole.

Bedding dips were picked on both oriented-core and BHTV images by fitting sinusoids along observed bedding planes. The core picks are sensitive to color changes, associated with mineralogic variations, whereas BHTV character is most sensitive to porosity and therefore to grain size. The core bedding picks are the most reliable of our three techniques, with minimal ambiguity about bedding *vs.* fractures. BHTV-based bedding analysis could be undertaken on a much larger percentage of the hole than that with oriented core, but we have confined our BHTV analyses to the same intervals as for oriented core. The core and BHTV picks were undertaken in parallel, using side-by-side images to increase confidence in bedding identifications.

BEDDING DIP RESULTS

A common approach to dipmeter analysis is to examine patterns within so-called “tadpole plots”, dip *vs.* depth plots in which dip azimuth is indicated by a short line segment on each data point. For each of the three CRP-3 bedding datasets (dipmeter, oriented-core, and BHTV), we have examined both tadpole plots and stereographic plots of poles to bedding, to identify intervals with uniform bedding behavior. The selection of intervals and their boundaries is based primarily on identification of sudden changes in average dip direction (dip magnitude or azimuth) on the tadpole and stereographic plots. Noise is subsequently minimized by considering interval means, with associated 95% confidence limits, rather than individual data points. Interval means are calculated by applying Fisher statistics, applicable to dispersion on a sphere, to the poles of bedding. This method provides an unbiased mean dip direction, whereas separate arithmetic averaging of dip directions and dip azimuths yields a biased mean dip direction, particularly for small dips.

Table 1 lists the abundances of bedding dip determinations, for the three stratigraphic zones (Tertiary shelf, dolerite breccia, and Beacon sandstone) and three methods (dipmeter, oriented-core, and BHTV). Our initial dataset of bedding orientations consists of 4286 dipmeter beds, 877 oriented-core beds, and 821 BHTV beds. During the process of interval identification, some data were omitted because they fell between intervals of uniform dip behavior. In addition, a few points were deleted from within some groups because their directions were dramatically different from those of the overall population. Percentages of deleted data and final data abundances are also listed in table 1.

Table 2 shows the dipmeter data intervals and interval-average bedding orientations. Also shown for each mean are the precision parameter k (larger values indicate higher precision) and the radius (in degrees) of the 95% confidence circle. Table 3 shows

Tab. 1 - Abundances of bedding picks.

<i>Zone</i>	<i>Method</i>	<i>Initial # points</i>	<i>% deleted: between groups</i>	<i>% deleted: within groups</i>	<i>Final # points</i>
<i>Tertiary shelf</i>	dipmeter	3772	2.6	2.0	3600
	oriented core	550	5.1	1.1	516
	BHTV	601	4.2	1.3	568
<i>dolerite breccia</i>	dipmeter	15	0	0	15
	oriented core	26	4	0	25
	BHTV	16	6	0	15
<i>Beacon</i>	dipmeter	499	0	1.2	493
	oriented core	301	7.3	3.3	274
	BHTV	204	0	6.9	185

corresponding results for oriented-core and BHTV dip orientations. Comparison of dip magnitudes for oriented-core and BHTV results for the same interval suggests that oriented-core dips are systematically about 3° steeper than BHTV dips; we cannot account for this discrepancy. Unlike oriented-core and BHTV results, adjacent dipmeter-based dip determinations are not independent, because Ezdip® uses an artificial intelligence algorithm to suppress inconsistent results (Kerzner, 1983, 1986, 1988) and because the step increment is shorter than the window length. Therefore, confidence limits are optimistic for interval-averaged dipmeter results.

All of the interval bedding orientations of tables 2 and 3 include structural dip, but many may also include a component of sedimentary dip, either depositional (*e.g.*, cross bedding) or post-depositional (*e.g.*, soft-sediment deformation). In order to isolate structural dip, we applied three exclusion criteria aimed at identifying intervals with detectable sedimentary dip effects. First and most important is recognition of a skewed distribution, either on a stereographic projection of bedding perpendiculars or on a tadpole plot. On a stereographic projection, parallel bedding generates a distribution that is approximately circular (*i.e.*, no dependence of standard deviation on azimuth), whereas cross bedding and soft-sediment deformation generate oval distributions that are strongly skewed (higher standard deviation) in the plane of cross bedding or soft-sediment movement. On a tadpole plot, sedimentary dips often generate a pattern of systematically increasing or decreasing dips over a ~2-20 m interval. Second, some intervals exhibited high data dispersion, usually due to sedimentary dips or – for dipmeter data – low coherence among traces. We exclude the highest-dispersion intervals, using an arbitrary threshold of ≥ 10 for the precision parameter k . Finally, some intervals have mean bedding directions that are anomalous in comparison with other mean results from the same broad portion of CRP-3. The most likely reason for these anomalous directions is either depositional or post-depositional sedimentary dip. In either case, these anomalous intervals are not representative of regional structural dip.

Tables 2 and 3 flag intervals that have skewed distributions, excessive scatter ($k < 10$), or anomalous directions, along with those that survive these three rejection criteria. Half of the 58 dipmeter-based dip directions for Tertiary shelf sediments are useful indicators of structural dip; only 3 of the 30 rejected intervals are excluded solely on the basis of anomalous directions. Similarly, half of the 40 oriented-core and BHTV dip directions for Tertiary shelf sediments were excluded, almost always because strong skewing indicates that these generally short (2-10 m) intervals are dominated by sedimentary dips. Only 1 of these rejected intervals is excluded solely based on an anomalous direction. The same criteria used to eliminate intervals with sedimentary dip are also useful in reducing dipmeter bias associated with fracturing and brecciation in the lower part of the drillhole. Of the 11 breccia and Beacon intervals (including two suites of Beacon results with different processing parameters), only 3 survive our exclusion criteria. Recognizing the superiority of oriented-core and BHTV over dipmeter for identification of bedding in the breccia and Beacon, we concentrated our oriented-core and BHTV analyses there. Of the 14 core and BHTV interval means from the breccia and Beacon, only 4 were rejected.

The methods of interval identification and averaging employed here are identical to those used for CRP-2A dipmeter analysis (Jarrard et al., 2000). The criteria for isolating structural dips by excluding sedimentary dips are different, however. Jarrard et al. (2000) identified five short intervals, of 31 total, as having anomalous directions when compared to adjacent intervals. Consequently, they excluded those intervals from their interpretations of structural dip variations. If, instead, one applies the three CRP-3 exclusion criteria, then 5 intervals (their intervals C, G, H, J, and O) are excluded because of skewed distributions, in addition to the 5 previously excluded because of anomalous directions.

Figure 1 shows mean dip directions for those Tertiary shelf intervals that appear to be reliable indicators of structural dip (Tabs. 1 & 2). All dip directions for 113-789 mbsf are consistent in indicating a uniform dip direction, with what appears

Tab. 2 - Interval-mean bedding directions based on dipmeter analyses.

Start depth	End depth	Zone	OK	skewed	scatter	anomalous	N	azi	dip	k	95%
20.8	23.1	shelf		X	X		9	52.6	12.9	7.6	18.7
24.3	34.0	shelf	X		6		5	72.2	23.1	17.9	4.3
34.2	39.6	shelf		X		X	35	244.0	17.5	13.7	6.8
40.0	53.3	shelf	X		7		3	124.3	7.6	11.7	5.1
53.4	58.5	shelf		X		X	33	275.4	26.0	15.1	6.7
61.0	76.5	shelf	X		9		2	128.6	7.9	10.5	4.8
77.1	83.2	shelf	X		5		2	71.8	11.1	140.1	1.7
86.0	93.9	shelf		X		X	29	253.8	30.0	20.7	6.0
94.3	112.3	shelf			X		57	34.1	13.1	7.3	7.5
113.3	127.6	shelf	X		7		1	70.2	19.8	16.3	4.3
128.7	144.5	shelf			X		59	91.5	17.0	9.2	6.4
152.8	163.5	shelf	X		6		6	45.3	24.0	16.1	4.5
170.7	181.1	shelf	X		6		5	76.6	17.6	10.4	5.7
181.5	211.2	shelf			X		133	19.1	11.9	9.4	4.2
214.3	234.8	shelf		X		7	9	59.4	23.6	13.2	4.6
239.3	255.1	shelf	X		6		6	70.3	19.3	15.3	4.6
272.3	285.1	shelf	X		6		9	76.2	18.7	12.0	5.2
285.3	287.2	shelf		X		X	10	210.1	16.4	26.6	9.0
287.5	293.0	shelf	X		2		4	70.4	20.9	15.3	7.8
303.4	317.6	shelf			X		75	85.3	14.0	8.6	5.9
318.8	325.1	shelf		X	X	X	15	318.6	13.9	7.7	14.1
325.2	337.9	shelf	X		8		8	52.7	19.4	13.2	4.3
338.2	347.9	shelf			X	X	46	319.3	14.3	8.5	7.7
348.3	366.2	shelf	X		1		10	83.9	22.2	10.9	4.3
367.2	389.6	shelf			X		83	62.8	11.8	7.6	6.0
390.0	394.2	shelf				X	27	340.1	24.8	11.5	8.6
394.3	405.0	shelf		X		4	4	70.7	13.1	10.4	7.0
405.1	414.3	shelf		X	X	X	44	184.6	3.4	7.4	8.5
415.8	424.5	shelf	X		5		2	79.2	22.9	21.2	4.4
424.7	460.1	shelf	X		1		64	66.9	14.8	13.6	3.1
460.6	463.4	shelf		X		X	33	267.9	19.5	14.9	6.7
463.6	476.9	shelf	X		1		09	42.6	21.4	10.1	4.5
481.3	488.3	shelf	X		5		5	47.7	25.0	24.2	4.0
489.0	518.5	shelf			X		126	58.3	13.8	9.9	4.2
518.6	525.2	shelf		X		X	46	3.0	21.5	17.7	5.1
525.2	528.5	shelf		X	X	X	20	338.4	8.7	8.0	12.3
528.6	554.8	shelf	X		1		28	64.3	22.4	12.7	3.6
555.2	560.3	shelf		X		4	7	81.9	18.3	34.6	3.6
563.7	574.5	shelf			X	X	54	169.2	5.5	8.7	7.0
579.1	588.1	shelf		X	X		30	67.9	23.7	8.5	9.6
588.3	592.0	shelf	X		2		6	71.9	24.3	28.5	5.4
593.3	596.4	shelf		X		X	13	266.1	6.3	10.6	12.8
597.6	604.0	shelf	X		4		1	74.1	18.2	14.3	6.1
605.4	624.0	shelf			X		87	26.0	5.0	7.2	6.1
624.3	634.0	shelf	X		6		8	44.6	22.0	21.8	3.8
634.6	639.8	shelf		X		5	0	103.6	15.6	22.4	4.4
643.1	660.6	shelf	X		1		10	42.0	19.1	22.7	2.9
660.7	671.0	shelf	X		1		03	71.6	27.4	22.4	3.0
671.2	686.0	shelf	X		1		19	71.3	23.9	14.2	3.6
689.4	702.1	shelf	X		5		6	77.4	13.9	11.7	5.8
703.4	725.6	shelf	X		1		01	51.1	17.5	20.8	3.2
729.3	750.2	shelf	X		1		50	55.4	22.0	29.7	2.1
750.3	752.6	shelf				X	21	328.1	29.9	45.7	4.8
753.0	763.4	shelf		X		5	7	53.8	19.9	15.7	4.9
764.4	765.6	shelf		X		X	11	329.6	10.6	18.9	10.3
765.7	769.7	shelf	X		6		4	88.5	23.5	23.4	3.7
770.9	771.7	shelf				X	10	332.9	20.1	86.9	4.9
777.9	791.2	shelf	X		4		9	63.4	24.0	15.2	5.4
793.6	822.6	breccia		X		1	5	43.1	22.4	15.8	9.6
827.7	838.2	Beacon1			X	X	11	167.3	4.3	8.5	15.8
838.4	847.4	Beacon1		X		1	6	36.2	19.9	54.3	5.1
847.9	872.7	Beacon1	X		5		1	17.4	11.4	48.6	2.9
874.1	900.1	Beacon1		X		6	0	79.6	4.1	12.2	5.5
825.9	831.4	Beacon2		X		X	29	315.9	16.2	19.0	6.3
832.4	841.3	Beacon2		X		3	9	99.5	3.6	14.1	6.3
841.6	849.8	Beacon2	X		3		8	32.8	18.5	23.7	4.9
850.1	855.6	Beacon2				X	18	303.8	18.3	24.8	7.1
856.1	871.3	Beacon2	X		7		6	34.4	9.9	27.0	3.2
871.5	900.1	Beacon2		X		1	55	63.2	3.6	13.3	3.2

Tab. 3 - Interval-mean bedding directions based on core-scan and borehole televiewer data.

zone	start depth	end depth	core								
			OK	skewed	scatter	anomalous	N	azi	dip	k	95%
shelf	404.3	408.8		X	X	X	21	228.8	31.1	4.0	18.2
shelf	410.3	413.5	X				26	79.6	23.8	44.1	4.3
shelf	451.6	452.8		X		X	7	318.6	30.8	13.1	16.0
shelf	455.4	460.1	X				44	78.7	18.9	51.1	3.0
shelf	460.2	463.2		X		X	14	263.9	17.3	14.7	10.3
shelf	541.2	548.5	X				9	72.7	22.6	56.5	6.5
shelf	555.8	561.6		X			50	108.1	17.9	25.8	4.0
shelf	574.8	578.1		X			26	53.4	26.4	10.5	9.2
shelf	578.0	587.2	X				42	66.0	25.3	53.3	3.0
shelf	616.2	620.2		X			12	50.0	22.1	18.8	9.8
shelf	624.1	634.1	X				54	66.6	25.5	18.9	4.6
shelf	642.1	657.2		X			38	96.8	24.2	10.9	7.4
shelf	658.3	660.6		X			18	106.4	14.9	89.9	3.7
shelf	661.0	666.5	X				43	78.3	24.5	34.8	3.7
shelf	693.4	697.6	X				26	83.4	27.0	81.0	3.2
shelf	697.6	698.6	X				21	34.1	24.2	135.0	2.7
shelf	701.4	704.7	X				5	78.4	23.2	34.9	11.7
shelf	704.8	713.1			X	X	33	8.0	7.3	6.2	11.0
shelf	714.0	720.2		X			16	75.5	22.1	25.9	7.4
shelf	722.2	723.7		X			11	101.6	19.1	16.4	11.0
shelf	750.2	768.9									
breccia	787.2	794.4	X				20	68.6	30.8	43.2	5.0
breccia	807.0	810.3		X			5	52.9	43.8	23.7	14.3
Beacon	823.1	829.4		X			103	57.0	23.3	111.2	1.3
Beacon	864.3	875.0	X				85	50.0	19.2	79.9	1.7
Beacon	875.0	881.2	X				27	79.3	29.1	48.6	4.0
Beacon	881.2	895.2		X			3	95.5	21.5	80.4	11.3
Beacon	895.2	904.2	X				56	108.2	23.6	114.7	1.8

zone	start depth	end depth	BHTV								
			OK	skewed	scatter	anomalous	N	azi	dip	k	95%
shelf	404.3	408.8		X	X	X	24	267.6	17.2	4.9	14.9
shelf	410.3	413.5	X				27	62.1	18.6	36.8	4.6
shelf	451.6	452.8									
shelf	455.4	460.1	X				34	70.8	16.5	73.5	2.9
shelf	460.2	463.2				X	11	245.4	16.7	15.8	11.3
shelf	541.2	548.5	X				12	80.2	15.9	58.6	5.5
shelf	555.8	561.6		X			36	99.6	17.3	27.2	4.7
shelf	574.8	578.1		X			22	39.0	22.2	11.8	9.4
shelf	578.0	587.2	X				29	57.5	19.6	83.1	3.0
shelf	616.2	620.2		X			12	77.5	21.1	33.3	7.3
shelf	624.1	634.1	X				45	73.1	21.5	21.4	4.7
shelf	642.1	657.2		X			47	83.4	17.2	16.1	5.3
shelf	658.3	660.6	X				17	100.4	14.6	67.0	4.4
shelf	661.0	666.5	X				59	75.6	22.2	55.1	2.5
shelf	693.4	697.6	X				28	70.5	21.1	54.3	3.7
shelf	697.6	698.6	X				22	25.6	21.2	133.9	2.7
shelf	701.4	704.7	X				23	53.6	23.6	38.8	4.9
shelf	704.8	713.1		X		X	42	17.3	8.9	12.6	6.5
shelf	714.0	720.2		X			23	61.7	17.0	56.1	4.1
shelf	722.2	723.7		X		X	15	134.8	3.2	13.1	10.6
shelf	750.2	768.9		X			40	91.4	13.1	24.4	4.7
breccia	787.2	794.4	X				10	77.7	29.9	35.0	7.8
breccia	807.0	810.3		X			5	48.7	38.8	18.0	16.5
Beacon	823.1	829.4	X				54	57.5	23.6	132.1	1.7
Beacon	864.3	875.0	X				51	61.6	15.9	134.6	1.7
Beacon	875.0	881.2	X				24	77.1	26.5	120.0	2.7
Beacon	881.2	895.2	X				34	78.7	18.9	97.5	2.5
Beacon	895.2	904.2	X				22	102.9	23.9	76.0	3.6

to be random dispersion of $<10^\circ$ about the average direction. Based on the 24 dipmeter-based results, with unit weight to each interval average, the overall mean dip direction for 113-789 mbsf is a dip of 20.5° toward azimuth 64.8° (95% confidence radius $\alpha_{95}=2.2^\circ$). This result is confirmed by oriented cores

(dip 23.2° , azimuth 71.0° , $\alpha_{95}=4.1^\circ$) and BHTV (dip 18.6° , azimuth 65.6° , $\alpha_{95}=4.1^\circ$) (Fig. 1). Data from shallower than ~ 100 m exhibit dip directions that appear to be a few degrees shallower, on average, than the mean for 113-789 mbsf, but too few intervals are available to quantify this shallowing.

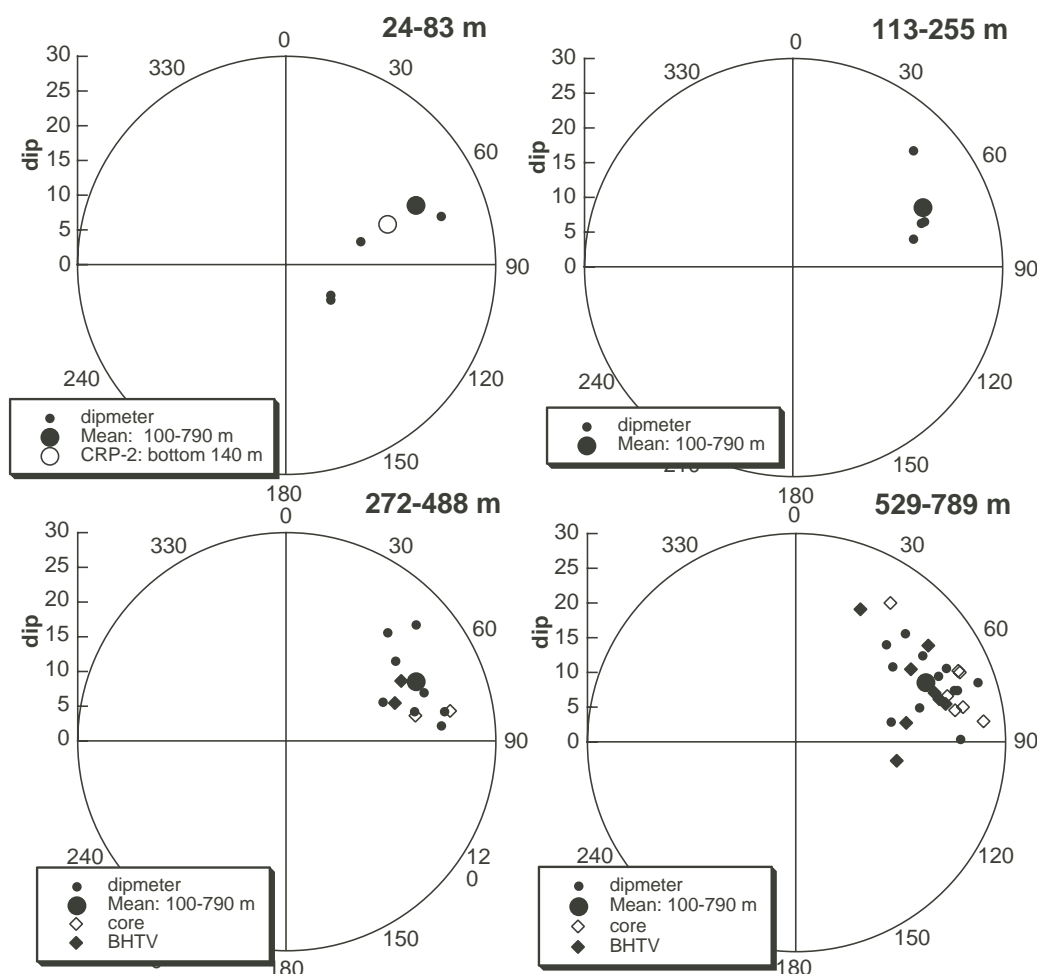


Fig. 1 - Interval mean dip directions for Tertiary shelf sediments of CRP-3, based on dipmeter (solid dots), core images (open diamonds), and borehole televier (solid diamonds). Results are listed in tables 1 & 2. Also shown are the mean structural dips for the lower portion of CRP-2A (Jarrard et al., 2000) and for most of CRP-3. In these zoomed polar projections, dip magnitude increases from zero at the center to 30° at the outer circle of each plot.

Figure 2 shows interval-mean bedding directions for the Beacon sandstone, based on oriented-core and BHTV bedding picks. Dipmeter results (Tab. 1), not shown here because they are probably biased by fractures and brecciation, are generally shallower and more northerly. Oriented-core and BHTV results for the same interval, connected by a line segment in figure 2, are consistently very similar. Dispersion among intervals is up to 20°. The overall average of these Beacon results is compatible with the shelf-sediment mean for the overlying interval 113-789 mbsf.

Figure 2 also shows individual bedding directions from within the doleritic breccia. These data are based only on oriented-core and BHTV picks, which are much more reliable than dipmeter-based results from this interval. Contamination of the dipmeter result by faulting gives it a skewed distribution and a mean dip magnitude (Tab. 1) much shallower than the oriented-core and BHTV results. The doleritic breccia has an average dip azimuth that is similar to the structural dip azimuths of the overlying shelf

sediments and underlying Beacon, but dips are about 10° steeper. We consider the most likely explanation of this dip steepening to be sedimentary dip, associated with interpreted (Cape Roberts Science Team, 2000) deposition on a subaerial fan. This bedding direction is approximately parallel to a faulting fabric identified in this portion of the doleritic breccia (Wilson & Paulsen, this volume). Although we can readily distinguish between bedding and open fractures in the core and BHTV images, it is conceivable that some or many of our “bedding” picks are actually calcite-filled fractures.

IMPLICATIONS FOR STRUCTURAL HISTORY

This portion of the Victoria Land basin is extensively faulted: three faults cut CRP-3 (Cape Roberts Science Team, 2000; Wilson & Paulsen, this volume), and at least two fault fabrics are evident on seismic reflection profiles (Hamilton et al., 1998) and at nearby Cape Roberts (Wilson, 1995). The CRP-3

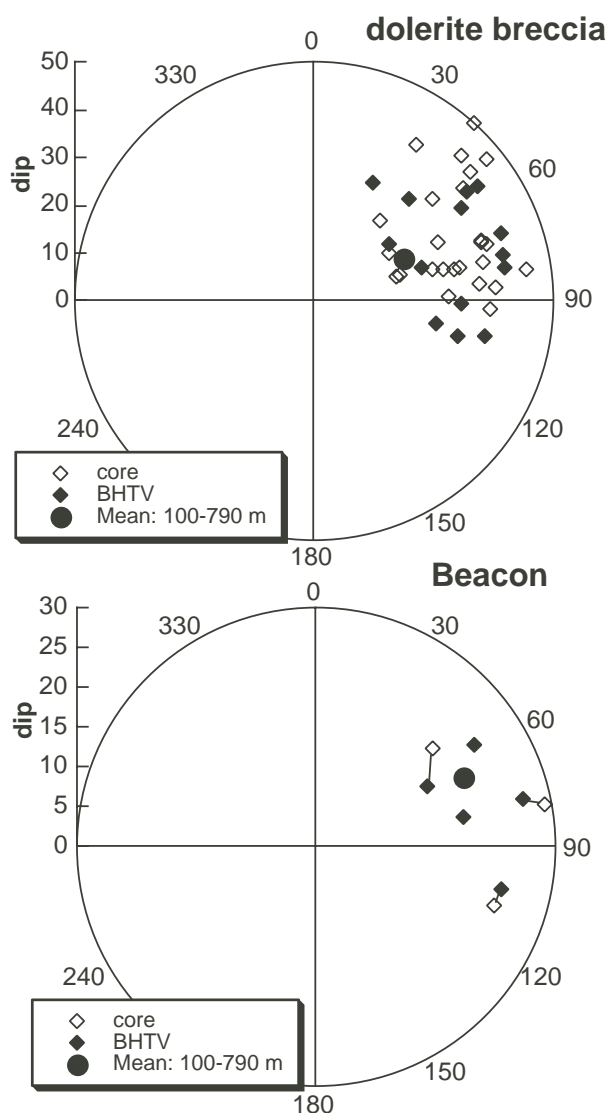


Fig. 2 - Polar projections of dip data for a dolerite breccia at 789-823 m (top) and underlying Devonian Beacon sandstone (bottom), compared to the mean result for overlying Tertiary shelf sediments. Dolerite breccia results for individual beds are systematically steeper than adjacent zones, probably because of sedimentary dips. Beacon mean results for five intervals detect no systematic tilting compared to overlying Tertiary shelf data.

interval 113-789 mbsf is shown as three polar plots in figure 1, separated by depths of faults recognized at 260 mbsf and 540 mbsf. No change in structural dip is detectable across these faults. Furthermore, neither interval means nor individual bedding dips adjacent to the faults exhibit the characteristic signature of normal-fault drag: systematically increasing dips as the fault is approached from either above or below. Faulting does not appear to have imparted nonrepresentative local dips at CRP: the 65° down-dip azimuth of CRP-3 and 75° azimuth of CRP-2A are compatible with 71° and 79° dip azimuths for the bases of V4 and V3 seismic reflectors, respectively, based on regional structure contour maps (Henry et al., 1998).

Although depth-dependent variations in dip can be identified in the polar plots for CRP-3 (Figs. 1 and 2) and CRP-2A (Jarrard et al., 2000), a plot of dip vs. depth may be more useful for this purpose. For structural interpretation, total dip is less relevant than dip in the plane of structural tilting. Consequently, for each CRP-3 interval mean from tables 2 and 3 identified as being representative of structural dip, we calculated the component of dip within a structural tilt plane with azimuth 65° . Oriented-core and BHTV tilts, which are paired for the same interval, were averaged. Figure 3 shows these dipmeter-based and core/BHTV-based estimates of tilt vs. composite stratigraphic depth. We use composite stratigraphic depth to permit inclusion of data from both CRP-2A and CRP-3. CRP-2A results (excluding low-reliability intervals identified above) employ a slightly different structural tilt azimuth of 75° (Jarrard et al., 2000). Positive values indicate "eastward" (actually towards 65° or 75°) tilt, and negative values indicate "westward" tilt.

Superimposed on our bedding results in figure 3 are the dips of seismic reflectors that intersect the drill sites (Henry et al., this volume). The seismic profile is migrated to minimize dip artifacts (Henry et al., this volume). The seismic and dipmeter tilt patterns are consistent at CRP-2A (Jarrard et al., 2000), but seismic tilts at CRP-3 are $\sim 6^\circ$ less than dipmeter and core/BHTV tilts. Seismic profiles underestimate true dip unless they parallel down-dip direction, but this correction is negligible at CRP-2 and only 0.25° at CRP-3. Although the reason for this discrepancy is not known, we suspect that all datasets are correct and that the discrepancy may be attributable to the fact that CRP-3 does not lie exactly on the seismic line.

The overall structural dip history of CRP (Fig. 3) is a pattern of structural stability during most of CRP-3 time (Early Oligocene), followed by rapid eastward tilting during CRP-2/2A time (Early Oligocene to Early Miocene). All data types agree that $\sim 0\text{-}3^\circ$ of tilting occurred within CRP-3 time and a further $\sim 10\text{-}15^\circ$ of tilting occurred within CRP-2A time. The episode of accelerated tilting is probably attributable to activity on an offshore growth fault, as no other subsidence mechanism can account for such a rapid lateral fanning of seismic reflectors. Seismic reflection profiling does detect a westward-dipping normal fault just east of CRP-1 (Hamilton et al., 1998).

Although the two shallowest dipmeter results from CRP-2A indicate dips of several degrees to the northwest, both seismic evidence and correlations between CRP-1 and CRP-2/2A (Cape Roberts Science Team, 2000) indicate an eastward dip of $\sim 5^\circ$ for this portion of CRP-2A. Therefore, these unconfirmed dipmeter results should be treated with caution.

A gradual downhole increase in dip throughout CRP-2A is demonstrated by both dipmeter and

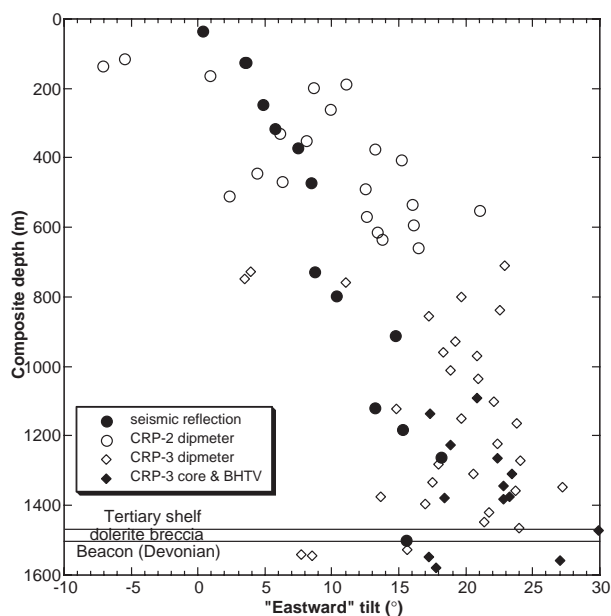


Fig. 3 - Mean dip directions for CRP-2A (Jarrard et al., 2000), CRP-3 (Tabs. 1 & 2), and a seismic reflection profile across these sites (Henry et al., this volume), displayed as a plot of "eastward" tilt versus composite stratigraphic depth. Each tilt is the dip component within the structural dip plane.

seismic results (Fig. 3) and confirmed by whole-core imaging (Jarrard et al., 2000). In contrast to the substantial local dip variations implied by CRP-2A dipmeter data, seismic dips exhibit a smooth, gradual increase downhole. This difference cannot be attributed to dipmeter picking error, as dip inhomogeneity is confirmed by core images. The large averaging volume of seismic profiling minimizes effects of sedimentary dip inhomogeneity, permitting structural dip to dominate. CRP-2A dipmeter data below 480 mbsf provide an average dip estimate of $15 \pm 2^\circ$.

Tilt is nearly constant at $20\text{--}22^\circ$, possibly with a downhole increase of $\sim 2^\circ$, throughout all but the topmost portion of the CRP-3 shelf sediments. The depth of transition from 15° to 21° dips is only approximately determined. The intervals above ~ 100 mbsf at CRP-3 have an intermediate average dip (Fig. 1), but dispersion is high, and too few intervals are available for discrimination. At CRP-2A, core dips increase to $20\text{--}30^\circ$ at the very bottom of the hole (605-625 mbsf), but this interval is short, soft-sediment deformation is locally evident, and dipmeter data do not provide confirmation.

ANGULAR UNCONFORMITIES

Several major unconformities have been identified at CRP, on the basis of biostratigraphic and other age data (Cape Roberts Science Team, 1999, 2000): 130 mbsf, 307 mbsf, and 443 mbsf at CRP-2/2A, and 823 mbsf at CRP-3. These depths correspond to 170, 347, 483, and 1503 m on the composite stratigraphic

section of figure 3. Structural dips from dipmeter, BHTV, core images, and seismic reflection provide evidence concerning which, if any, of these are angular unconformities.

Jarrard et al. (2000) conclude that CRP-2A dipmeter data are compatible with interpretation of the 130 mbsf unconformity as an angular unconformity, but the results are not compelling. The major unconformity at about 306 mbsf is not evident as an angular unconformity in the dipmeter data, but core dips may indicate a sudden dip increase at 297 mbsf. Dipmeter data indicate a steepening of dip within the 435-481 mbsf interval bracketing the 443 mbsf unconformity, but core dips do not confirm this observation.

The 823 mbsf CRP-3 unconformity separating the Early Oligocene and Devonian marks the initial rifting of this part of Victoria Land basin. Rifting has dropped these Devonian Beacon sandstones about 3 km below their lateral equivalents (Cape Roberts Science Team, 2000), mostly accommodated on a boundary fault 8 km west of CRP-3 (Hamilton et al., 1998; Henry et al., 1998). Large-offset normal faults are usually not planar, but concave and often listric. Therefore, the Tertiary/Devonian boundary at CRP-3 is expected to be an angular unconformity, with shallower dips for the Devonian than for overlying Tertiary shelf sediments. The three Beacon dipmeter data do suggest this pattern (Fig. 3), but the much more reliable oriented-core and BHTV dip data demonstrate that no significant angular unconformity is present (Figs. 2 & 3). Because the Beacon sandstone is intensely faulted and brecciated at CRP-3, we cannot exclude the hypothesis that CRP-3 is nonrepresentative of wider-scale Beacon structural dips.

ACKNOWLEDGEMENTS - This research was supported by the National Science Foundation (OPP-9527319 and OPP-9517394). We thank Alex Pyne for optimizing logging conditions.

REFERENCES

- Bücker C.J., Jarrard R.D. & Wonik T., 2001. Downhole temperature, radiogenic heat production, and heat flow from the CRP-3 drillhole, Victoria Land Basin, Antarctica. This volume.
- Bücker C.J., Jarrard R.D., Niessen F. & Wonik T., 2001. Statistical analysis of wireline logging data the CRP-3 drillhole, Victoria Land, Antarctica. This volume.
- Cape Roberts Science Team, 1999. Studies from the Cape Roberts Project, Ross Sea, Antarctica, Initial Report on CRP-2/2A. *Terra Antarctica*, 6, 1-173.
- Cape Roberts Science Team, 2000. Studies from the Cape Roberts Project, Ross Sea, Antarctica, Initial Report on CRP-3. *Terra Antarctica*, 7, 1-209.

- Hamilton R.J., Sorlien C.C., Luyendyk B.P., Bartek L.R. & Henrys S.A., 1998. Tectonic regimes and structural trends off Cape Roberts, Antarctica. *Terra Antartica*, **5**, 261-272.
- Henrys S.A., Bartek L.R., Brancolini G., Luyendyk B.P., Hamilton R.J., Sorlien C.C. & Davey F.J., 1998. Seismic stratigraphy of the pre-Quaternary strata off Cape Roberts and their correlation with strata cored in the CIROS-1 drillhole, McMurdo Sound. *Terra Antartica*, **5**, 273-279.
- Henrys S.A., Bucker C.J., Niessen F. & Bartek L.R., 2001. Correlation of seismic reflectors with the CRP-3 drillhole, Victoria Land Basin, Antarctica. This volume.
- Jarrard R.D., Brink J.D., Bucker C., Wonik T., Wilson T.J. & Paulsen T.S., 2000. Bedding dips in CRP-2A, Victoria Land Basin, Antarctica. *Terra Antartica*, **7**, 261-270.
- Jarrard R.D., Paulsen T.S. & Wilson T.J., 2001. Orientation of CRP-3 core, Victoria Land Basin, Antarctica. This volume.
- Jarrard R.D., Moos D., Wilson T.J., Bucker C.J. & Paulsen T.S., 2001. Stress patterns observed by borehole televiewer logging of the CRP-3 drillhole, Victoria Land Basin, Antarctica. This volume.
- Kerzner M.G., 1983. Formation dip determination - an artificial intelligence approach. *Log Analyst*, **24**, 10-22.
- Kerzner M.G., 1986. *Image Processing in Well Log Analysis*, IHRDC, Boston.
- Kerzner M.G., 1988. A rule-based approach to dipmeter processing. *SPE*, paper 18128.
- Wilson T.J., 1995. Cenozoic transtension along the Transantarctic Mountains - West Antarctic Rift boundary, Southern Victoria Land, Antarctica. *Tectonics*, **14**, 531-545.
- Wilson T.J. & Paulsen T.S., 2001. Fault and fracture patterns in CRP-3 core, Victoria Land Basin, Antarctica. This volume.
- Zemanek J. Glenn E.E., Norton L.J. & Caldwell R.L., 1970. Formation evaluation by inspection with the borehole televiewer. *Geophysics*, **35**, 254-269.